Towards Understanding Mechanisms Governing Cytotoxicity of Metal Oxides Nanoparticles: Hints from Nano-QSAR Studies

A. Gajewicz[a], N. Schaeublin[b], B. Rasulev[c], S. Hussain[b], D. Leszczynska[d], T. Puzyn[a] and J. Leszczynski[c*]

[a] *Laboratory of Environmental Chemometrics, Institute for Environmental and Human Health Protection, Faculty of Chemistry, University of Gdańsk, Gdańsk, Poland*
[b] *Biological Interaction of Nanomaterials, Applied Biotechnology Branch, Human Effectiveness Directorate 711th, Human Performance Wing, Air Force Research Laboratory, Wright Patterson Air Force Base OH, USA*
[c] *Interdisciplinary Nanotoxicity Center, Department of Chemistry and Biochemistry, Jackson State University, Jackson MS, USA*
[d] *Interdisciplinary Nanotoxicity Center, Department of Civil and Environmental Engineering Jackson State University, Jackson MS, USA*

Supplementary material

*Corresponding author phone :phone: +1 601 979 3723; fax: +1 601 979 7823; e-mail: jerzy@icnanotox.org

Symbols and definitions of all calculated molecular descriptors

TABLE S1

Symbol	Definition of molecular descriptor	Included in the model?
QUANTUM - MECHANICAL DESCRIPTORS		
ΔH_f^c	**Standard enthalpy of formation of metal oxide nanocluster**	**Yes**
TE	Total energy	No
EE	Electronic energy	No
Core	Core–core repulsion energy	No
SAS	Solvent accessible surface	No
HOMO	Energy of the Highest Occupied Molecular Orbital	No
LUMO	Energy of the Lowest Unoccupied Molecular Orbital	No
η	Chemical hardness	No
S	Total softness	No
E_g	HOMO-LUMO energy gap	No
μ	Electronic chemical potential	No
E_V	Valance band	No
E_C	Conduction band	No
χ^c	**Mulliken's electronegativity**	**Yes**
Hard	Parr and Pople's absolute hardness	No
Shift	Schuurmann MO shift alpha	No
Ahof	Polarizability derived from the heat of formation	No
Ad	Polarizability derived from the dipole moment	No
IMAGE DESCRIPTORS		
A	Area	No
V	Volume	No
d_S	Surface diameter	No
$d_{V/m}$	Volume/mass diameter	No
d_{Sauter}	Volume/surface diameter	No
A_{R_x}	Aspect ratio X	No
A_{R_y}	Aspect ratio Y	No
P_X	Porosity X	No
P_Y	Porosity Y	No
Ψ	Sphericity	No
f_{circ}	Circularity	No

Crystallographic data utilized to construct the metal oxides clusters

TABLE S2

Metal oxide	Reference
Al_2O_3	Kondo, S., Tateishi K., Ishizawa N., *Structural Evolution of Corundum at High Temperatures.* Japanese Journal of Applied Physics, 2008. **47**: p. 616-619
Bi_2O_3	Cornei, N., Tancret N., Abraham F., Mentré O., New epsilon-Bi2O3 metastable polymorph. Inorganic Chemistry, 2006. **26**: p. 4886-4888.
CoO	Saito, S., Nakahigashi K., Shimomura Y., X-Ray Diffraction Study on CoO. Journal of the Physical Society of Japan, 1966. **21**: p. 850-860.
Cr_2O_3	Finger, L.W., Hazen R.M., Crystal structure and isothermal compression of Fe2O3, Cr2O3, and V2O3 to 50 kbars Journal of Applied Physics, 1980. **51**: p. 5362-5368
Fe_2O_3	Hill, A.H., Jiao F., Bruce P.G., Harrison A., Kockelmann W., Ritter C., Neutron Diffraction Study of Mesoporous and Bulk Hematite, α-Fe2O3. Chemistry of Materials, 2008. **20**: p. 4891–4899.
In_2O_3	Prewitt, C.T., Shannon R.D., Rogers D.B., The C Rare Earth Oxide-Corundum Transition and Crystal Chemistry of Oxides Having the Corundum Structure. Inorganic Chemistry, 1969. **8**: p. 1985-1993.
La_2O_3	Wu, B., Zinkevich M., Aldinger F., Wen D., Chen L., Ab initio study on structure and phase transition of A- and B-type rare-earth sesquioxides Ln2O3 (Ln=La–Lu, Y, and Sc) based on density function theory. Journal of Solid State Chemistry, 2007. **180**: p. 3280-3287.
Mn_2O_3	Norrestam, R., Ingri N., Östlund E., Bloom G., Hagen G., alpha-Manganese(III) Oxide --- a C-Type Sesquioxide of Orthorhombic Symmetry Acta Chemica Scandinavica, 1967. **21**: p. 2871-2884.
NiO	Shimomura, Y., Kojima M., Saito S., Crystal structure of ferromagnetic nickel oxide. Journal of the Physical Society of Japan, 1956. **11**: p. 1136-1146.
Sb_2O_3	Whitten, A.E., Dittrich B., Spackman M.A., Turner P., Brown T.C., Charge density analysis of two polymorphs of antimony(III) oxide. Dalton Transactions, 2004. **7**: p. 23-29.
SiO_2	Martinez, J.R., Palomares-Sanchez S., Ortega-Zarzosa G., Ruiz F., Chumakov Y., Rietveld refinement of amorphous SiO2 prepared via sol–gel method. Materials Letters, 2006. **60**: p. 3526–3529.
SnO_2	Gracia, L., Beltrán A., Andrés J., Characterization of the high-pressure structures and phase transformations in SnO2. A density functional theory study. The Journal of Physical Chemistry B, 2007. **111**: p. 6479-6485.
TiO_2	Swamy, V., Dubrovinsky L.S., Dubrovinskaia N.A., Langenhorst F., Simionovici A.S., Drakopoulos M., Dmitriev V., Weber H.P., Size effects on the structure and phase transition behavior of baddeleyite TiO2. Solid State Communications, 2005. **134**: p. 541–546.
V_2O_3	Rozier, P., Ratuszna A., Galy J., Comparative structural and electrical studies of V2O3 and V2-xNixO3 (0<x<0.75) solid solution. Zeitschrift fur Anorganische und Allgemeine Chemie, 2002. **628**: p. 1236-1242.
WO_3	Woodward, P.M., Sleight A.W., Vogt T., Ferroelectric Tungsten Trioxide Journal of Solid State Chemistry, 1997. **131**: p. 9-17.
Y_2O_3	Santos, C., Strecker K., Suzuki P.A., Kycia S., Silva O.M.M., Silva C., Stabilization of alpha-SIALONs using a rare-earth mixed oxide (RE2O3) as sintering additive. Materials Research Bulletin, 2005. **40**: p. 1094-1103.
ZnO	Singhal, R.K., Samariya A., Xing Y.-T., Kumar S., Dolia S.N., Deshpande U.P., Shripathi T., Saitovitch E.B., *Electronic and magnetic properties of Co-doped Zn O diluted magnetic semiconductor.* The Journal of Alloys and Compounds, 2010. **496**: p. 324-330.
ZrO_2	Naray-Szabo, S., *Zur Struktur des Baddeleyits ZrO2.* Zeitschrift fuer Kristallographie, Kristallgeometrie, Kristallphysik, Kristallchemie, 1936. **94**: p. 414-416.

List of calculated quantum - mechanical descriptors

TABLE S3

Metal oxide	ΔH_f^c	TE	EE	Core	SAS	HOMO	LUMO	η	S	E_g	μ	E_V	E_C	χ^c	Hard	Shift	Ahof	Ad	Metal oxide
	kcal/mol	eV	eV	eV	A^2	eV	eV	eV	eV	eV	eV	eV	eV	eV	eV	eV	A^3	A^3	
Al_2O_3	-600.0	-2755.8	-11997.7	9242.0	307.16	-8.53	1.66	-5.09	-0.10	-10.18	-3.44	1.66	-8.53	3.44	5.09	-3.44	17.83	17.79	Al_2O_3
Bi_2O_3	-148.5	-2864.3	-11242.7	8378.4	251.06	-9.43	-1.25	-4.09	-0.12	-8.18	-5.34	-1.25	-9.43	5.34	4.09	-5.34	19.92	19.84	Bi_2O_3
CoO	-786.8	-5378.2	-45466.7	40088.5	347.56	-9.21	-5.67	-1.77	-0.28	-3.55	-7.44	-5.67	-9.21	7.44	1.50	-8.25	45.50	45.50	CoO
Cr_2O_3	-235.3	-2507.8	-10028.3	7520.4	167.30	-8.25	-0.46	-3.89	-0.13	-7.79	-4.36	-0.46	-8.25	4.36	3.89	-4.36	16.35	16.02	Cr_2O_3
Fe_2O_3	-378.5	-3480.9	-13651.6	10170.7	172.57	-8.33	-0.09	-4.12	-0.12	-8.24	-4.21	-0.09	-8.33	4.21	4.44	-4.57	12.33	12.32	Fe_2O_3
In_2O_3	-52.1	-1961.0	-6085.1	4124.1	191.20	-10.62	-2.95	-3.84	-0.13	-7.68	-6.78	-2.95	-10.62	6.78	3.84	-6.78	12.44	12.43	In_2O_3
La_2O_3	-157.7	-2486.1	-8602.4	6116.2	232.92	-10.91	-2.00	-4.45	-0.11	-8.90	-6.45	-2.00	-10.91	6.45	4.45	-6.45	4.95	4.95	La_2O_3
Mn_2O_3	-96.3	-5269.3	-34774.7	29505.4	321.38	-5.02	-4.98	-0.02	-27.78	-0.04	-5.00	-4.98	-5.02	5.00	0.02	-5.00	734.03	40.97	Mn_2O_3
NiO	68.0	-4671.0	-22764.2	18093.2	179.35	-7.78	-1.16	-3.31	-0.15	-6.62	-4.47	-1.16	-7.78	4.47	3.04	-4.37	21.35	21.23	NiO
Sb_2O_3	-206.7	-2504.8	-10756.3	8251.5	255.24	-7.96	-0.96	-3.50	-0.14	-7.00	-4.46	-0.96	-7.96	4.46	3.50	-4.46	23.21	23.12	Sb_2O_3
SiO_2	-618.3	-2764.2	-10201.7	7437.6	262.92	-7.90	0.28	-4.09	-0.12	-8.18	-3.81	0.28	-7.90	3.81	4.09	-3.81	31.58	31.54	SiO_2
SnO_2	-266.6	-3511.0	-17713.0	14202.0	359.32	-6.97	-2.18	-2.40	-0.21	-4.79	-4.57	-2.18	-6.97	4.57	2.40	-4.57	34.22	34.14	SnO_2
TiO_2	-1492.0	-2782.9	-12685.1	9902.2	271.58	-7.08	-2.73	-2.18	-0.23	-4.36	-4.91	-2.73	-7.08	4.91	2.14	-4.33	49.54	24.94	TiO_2
V_2O_3	-139.5	-2168.1	-7623.9	5455.8	206.12	-5.81	-0.66	-2.58	-0.19	-5.15	-3.24	-0.66	-5.81	3.24	2.58	-3.24	26.36	26.22	V_2O_3
WO_3	-715.4	-4310.9	-21750.8	17439.9	302.37	-6.84	-6.61	-0.11	-4.41	-0.23	-6.73	-6.61	-6.84	6.73	0.11	-6.73	40.16	39.79	WO_3
Y_2O_3	-135.3	-2179.8	-9171.1	6991.3	636.97	-5.19	-1.51	-1.84	-0.27	-3.68	-3.35	-1.51	-5.19	3.35	1.84	-3.35	107.00	106.98	Y_2O_3
ZnO	-449.4	-1320.2	-3221.7	1901.5	153.42	-11.36	-5.30	-3.03	-0.16	-6.07	-8.33	-5.30	-11.36	8.33	3.03	-8.33	9.09	9.07	ZnO
ZrO_2	-638.1	-1331.3	-3510.7	2179.4	178.99	-10.92	1.03	-5.97	-0.08	-11.95	-4.95	1.03	-10.92	4.95	5.97	-4.95	10.74	10.71	ZrO_2

List of calculated image descriptors

TABLE S4

Metal oxide	A	V	$d_s = \sqrt{\frac{A}{\pi}}$	$d_{V/m} = \sqrt[3]{\frac{6V}{\pi}}$	$d_{Sauter} = \frac{6V}{A}$	$A_{R\_x} = \frac{d_{\min\_x}}{d_{\max\_y}}$	$A_{R\_y} = \frac{d_{\min\_y}}{d_{\max\_x}}$	$P_x = \sum_{i=1}^{n} \lvert x_i - x_j \rvert$	$P_y = \sum_{i=1}^{n} \lvert y_i - y_j \rvert$	$\psi = \frac{\pi^{1/3} 6V^{2/3}}{A}$	$f_{circ} = \frac{4\pi A}{V^2}$	Metal oxide
	Area	Volume	Surface diameter	Volume/ mass diameter	Volume/surface diameter	Aspect ratio X	Aspect ratio Y	Porosity X	Porosity Y	Sphericity	Circularity	
	[px]	[px]	$[(px)^{1/2}]$	$[(px)^{1/3}]$	[-]	[-]	[-]	[px]	[px]	$[(px)^{-1/3}]$	[1/px]	
Al_2O_3	1.11E+09	1.86E+06	1.88E+04	153	1.01E-02	0.568	0.072	5.15E+04	-3.16E+05	6.62E-05	4.00E-03	Al_2O_3
Bi_2O_3	9.80E+08	2.05E+06	1.77E+04	158	1.25E-02	0.402	0.055	-2.86E+05	-1.80E+05	7.94E-05	2.90E-03	Bi_2O_3
CoO	1.14E+09	2.14E+06	1.90E+04	160	1.13E-02	0.429	0.061	2.11E+04	-2.42E+05	7.07E-05	3.10E-03	CoO
Cr_2O_3	8.70E+08	1.52E+06	1.67E+04	143	1.05E-02	0.263	0.060	-3.42E+05	-5.51E+05	7.34E-05	4.70E-03	Cr_2O_3
Fe_2O_3	1.09E+09	1.78E+06	1.86E+04	150	9.80E-03	0.446	0.066	-1.18E+05	-3.18E+05	6.52E-05	4.30E-03	Fe_2O_3
In_2O_3	1.07E+09	2.04E+06	1.85E+04	157	1.14E-02	0.499	0.065	-1.68E+04	-2.81E+05	7.24E-05	3.20E-03	In_2O_3
La_2O_3	1.10E+09	1.91E+06	1.87E+04	154	1.05E-02	0.524	0.072	1.33E+04	-2.87E+05	6.79E-05	3.80E-03	La_2O_3
Mn_2O_3	1.09E+09	2.04E+06	1.86E+04	157	1.12E-02	0.479	0.064	7.57E+04	-2.46E+05	7.12E-05	3.30E-03	Mn_2O_3
NiO	1.19E+09	1.96E+06	1.95E+04	155	9.90E-03	0.596	0.068	6.55E+03	-3.11E+05	6.36E-05	3.90E-03	NiO
Sb_2O_3	9.60E+08	1.80E+06	1.74E+04	151	1.13E-02	0.241	0.055	3.49E+05	-3.72E+05	7.48E-05	3.70E-03	Sb_2O_3
SiO_2	9.70E+08	1.81E+06	1.76E+04	15	1.12E-02	0.421	0.065	1.25E+05	-4.13E+05	7.39E-05	3.70E-03	SiO_2
SnO_2	9.30E+08	1.68E+06	1.72E+04	148	1.09E-02	0.408	0.078	-6.23E+04	-4.28E+05	7.37E-05	4.10E-03	SnO_2
TiO_2	9.20E+08	1.77E+06	1.71E+04	150	1.16E-02	0.408	0.078	9.79E+03	-3.98E+05	7.70E-05	3.70E-03	TiO_2
V_2O_3	1.30E+09	2.20E+06	2.03E+04	161	1.02E-02	0.569	0.059	-5.81E+03	-2.20E+05	6.29E-05	3.40E-03	V_2O_3
WO_3	9.80E+08	1.72E+06	1.76E+04	149	1.06E-02	0.409	0.067	-1.67E+05	-4.30E+05	7.11E-05	4.10E-03	WO_3
Y_2O_3	1.28E+09	2.26E+06	2.02E+04	163	1.06E-02	0.633	0.058	1.02E+04	-1.89E+05	6.51E-05	3.10E-03	Y_2O_3
ZnO	1.11E+09	1.95E+06	1.88E+04	155	1.05E-02	0.535	0.071	1.83E+03	-3.04E+05	6.80E-05	3.70E-03	ZnO
ZrO_2	1.20E+09	2.22E+06	1.95E+04	162	1.11E-02	0.508	0.059	9.68E+03	-2.19E+05	6.86E-05	3.10E-03	ZrO_2

* [px] - number of pixels

	Name	Definition of image descriptor*	
Descriptors reflecting nanoparticle size	Volume (V)	The sum of all non-zero pixels episodes, combining measures of contour elements, assuming that the contour is a square with a side equal to the unity	
	Surface diameter (d_s)	The diameter of a sphere having the same surface area as the projected particle	$d_s = \sqrt{\frac{A}{\pi}}$
	Equivalent volume diameter (d_v)	The diameter of a sphere having the same volume as the projected particle	$d_{V/m} = \sqrt[3]{\frac{6V}{\pi}}$
	Equivalent volume/surface (d_{Sauter})	The diameter of a sphere having the same volume to surface ratio as the projected particle	$d_{Sauter} = \frac{6V}{A}$
Descriptors reflecting nanoparticle surface area	Area (A)	The sum of the all non-zero pixels (xi)	$A = \sum_{i=1}^{n} (x_i)$
	Porosity (P_x)	The sum of the relative differences in intensities between values of neighboring pixels (x_i and y_i) along the X axis	$P_x = \sum_{i=1}^{n} \lvert x_i - x_j \rvert$
	Porosity (P_y)	The sum of the relative differences in intensities between values of neighboring pixels (xi and yi) along the Y axis	$P_y = \sum_{i=1}^{n} \lvert y_i - y_j \rvert$
Descriptors reflecting nanoparticle shape	Sphericity (Ψ)	The ratio of the surface area of a sphere - with the same volume as the particle considered - to the surface area of the particle	$\psi = \frac{\pi^{1/3} 6V^{2/3}}{A}$
	Circularity (f_{circ})	The function of the surface area of the particle (A) and the particle's perimeter (V^2)	$f_{circ} = \frac{4\pi A}{V^2}$
	Anisotropy ratio (AR_x)	The ratio of the minimum length of chord of the X axis and the maximum length of chord of the Y axis.	$A_{R\_x} = \frac{d_{\min\_x}}{d_{\max\_y}}$
	Anisotropy ratio (AR_y)	The ratio of the minimum length of chord of the Y axis and the maximum length of chord of the X axis.	$A_{R\_y} = \frac{d_{\min\_y}}{d_{\max\_x}}$

* Javad Sameni, Particle size analysis - Pharmaceutical material and product characterization. Available from: http://www.authorstream.com/Presentation/javadsameni-231114-particle-size-analysis-pharmaceutics-particles-science-technology-ppt-powerpoint/ (accessed April 02, 2013).

Statistics for the model's coefficients

TABLE S5

		b_i	std. error	t-value	p-value
b_0	intercept	2.47	± 0.05	54.19	1.9×10^{-10}
b_1	coefficient	0.24	± 0.05	5.08	1.4×10^{-3}
b_2	coefficient	0.39	± 0.05	8.21	7.7×10^{-5}

Results for internal validation with leave-one-out algorithm

TABLE S6

			b_i	std. error	t-value	p-value	R^2	$RMSE_C$
Model CV-LOO$_{-1}$	b_0	intercept	2.54	± 0.05	49.26	4.7×10^{-9}	0.90	0.13
	b_1	coefficient	0.14	± 0.06	2.52	4.5×10^{-2}		
	b_2	coefficient	0.41	± 0.06	7.30	3.4×10^{-4}		
			b_i	std. error	t-value	p-value	R^2	$RMSE_C$
Model CV-LOO$_{-2}$	b_0	intercept	2.52	± 0.04	64.30	9.5×10^{-10}	0.95	0.10
	b_1	coefficient	0.24	± 0.04	5.85	1.1×10^{-3}		
	b_2	coefficient	0.41	± 0.04	9.76	6.7×10^{-5}		
			b_i	std. error	t-value	p-value	R^2	$RMSE_C$
Model CV-LOO$_{-3}$	b_0	intercept	2.50	± 0.05	52.73	3.1×10^{-9}	0.93	0.12
	b_1	coefficient	0.26	± 0.05	5.23	2.0×10^{-3}		
	b_2	coefficient	0.41	± 0.05	8.11	1.9×10^{-4}		
			b_i	std. error	t-value	p-value	R^2	$RMSE_C$
Model CV-LOO$_{-4}$	b_0	intercept	2.49	± 0.05	53.34	2.9×10^{-9}	0.94	0.11
	b_1	coefficient	0.23	± 0.05	4.72	3.3×10^{-3}		
	b_2	coefficient	0.40	± 0.05	7.96	2.1×10^{-4}		
			b_i	std. error	t-value	p-value	R^2	$RMSE_C$
Model CV-LOO$_{-5}$	b_0	intercept	2.48	± 0.05	48.65	5.1×10^{-9}	0.93	0.13
	b_1	coefficient	0.26	± 0.05	4.76	3.1×10^{-3}		
	b_2	coefficient	0.40	± 0.05	7.46	3.0×10^{-4}		
			b_i	std. error	t-value	p-value	R^2	$RMSE_C$
Model CV-LOO$_{-6}$	b_0	intercept	2.46	± 0.05	50.46	4.1×10^{-9}	0.94	0.12
	b_1	coefficient	0.26	± 0.05	5.05	2.3×10^{-3}		
	b_2	coefficient	0.42	± 0.05	8.06	2.0×10^{-4}		
			b_i	std. error	t-value	p-value	R^2	$RMSE_C$
Model CV-LOO$_{-7}$	b_0	intercept	2.45	± 0.05	48.50	5.2×10^{-9}	0.93	0.12
	b_1	coefficient	0.24	± 0.05	4.46	4.3×10^{-3}		
	b_2	coefficient	0.42	± 0.05	7.82	2.3×10^{-4}		
			b_i	std. error	t-value	p-value	R^2	$RMSE_C$
Model CV-LOO$_{-8}$	b_0	intercept	2.43	± 0.05	47.38	5.9×10^{-9}	0.92	0.13
	b_1	coefficient	0.26	± 0.05	4.69	3.4×10^{-3}		
	b_2	coefficient	0.37	± 0.05	6.73	5.2×10^{-4}		
			b_i	std. error	t-value	p-value	R^2	$RMSE_C$
Model CV-LOO$_{-9}$	b_0	intercept	2.42	± 0.05	49.19	4.7×10^{-9}	0.93	0.12
	b_1	coefficient	0.26	± 0.05	4.93	2.6×10^{-3}		
	b_2	coefficient	0.41	± 0.05	7.84	2.3×10^{-4}		
			b_i	std. error	t-value	p-value	R^2	$RMSE_C$
Model CV-LOO$_{-10}$	b_0	intercept	2.37	± 0.05	52.40	3.2×10^{-9}	0.91	0.11
	b_1	coefficient	0.26	± 0.05	5.30	1.8×10^{-3}		
	b_2	coefficient	0.28	± 0.05	5.85	1.1×10^{-3}		

The results of the Y-scrambling test

FIGURE S1

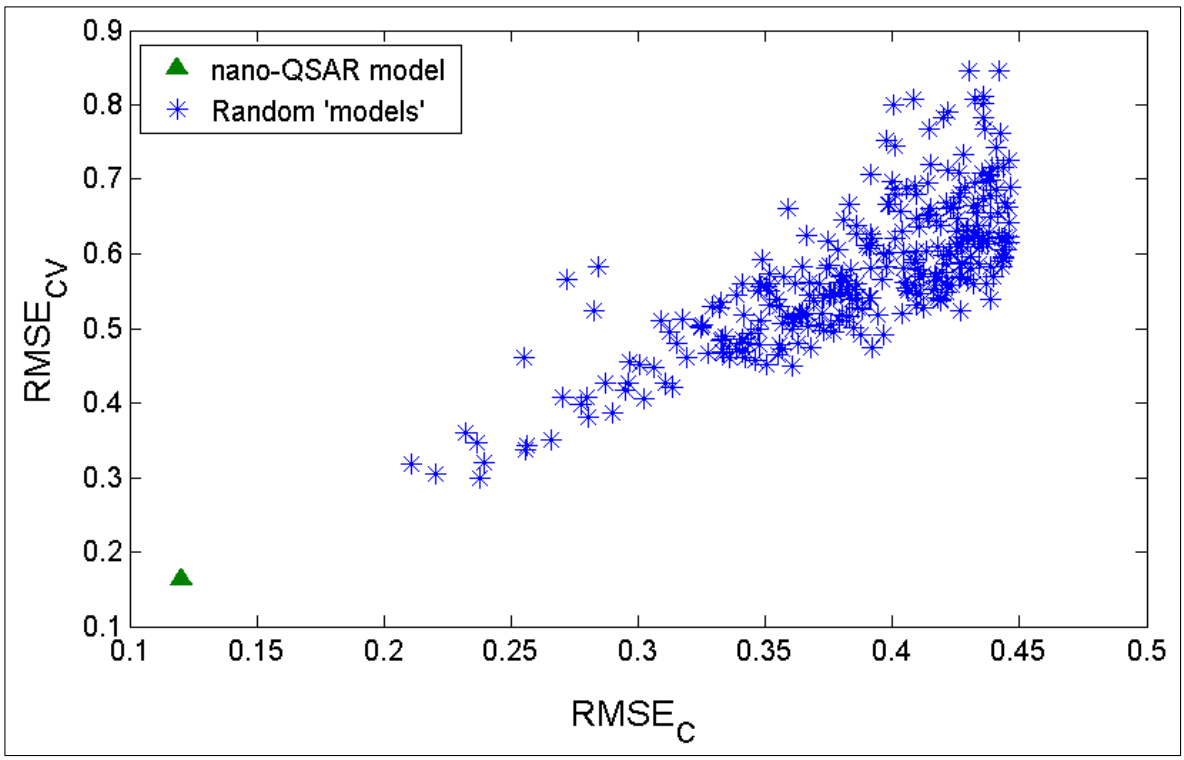

Insubria plot

FIGURE S2